Nonthermal Electron Energization from Magnetic Reconnection in Laser-Driven Plasmas

Samuel R. Totorica, Tom Abel, and Frederico Fiuza

Non-Thermal Electron Energization from Magnetic Reconnection in Laser-Driven Plasmas

S. Totorica,[1] T. Abel,[1] and F. Fiuza[2, *]

[1]*Kavli Institute for Particle Astrophysics and Cosmology, Stanford University,*
SLAC National Accelerator Laboratory, Menlo Park, CA 94025, USA
[2]*SLAC National Accelerator Laboratory, Menlo Park, CA 94025, USA*

(Dated: February 8, 2016)

Abstract

The possibility of studying non-thermal electron energization in laser-driven plasma experiments of magnetic reconnection is studied using two- and three-dimensional particle-in-cell simulations. It is demonstrated that non-thermal electrons with energies more than an order of magnitude larger than the initial thermal energy can be produced in plasma conditions currently accessible in the laboratory. Electrons are accelerated by the reconnection electric field, being injected at varied distances from the X-points, and in some cases trapped in plasmoids, before escaping the finite-sized system. Trapped electrons can be further energized by the electric field arising from the motion of the plasmoid. This acceleration gives rise to a non-thermal electron component that resembles a power-law spectrum, containing up to $\sim 8\%$ of the initial energy of the interacting electrons and $\sim 24\%$ of the initial magnetic energy. Estimates of the maximum electron energy and of the plasma conditions required to observe suprathermal electron acceleration are provided, paving the way for a new platform for the experimental study of particle acceleration induced by reconnection.

PACS numbers: 52.72.+v, 52.35.Vd, 41.75.Jv, 52.65.Rr

Magnetic reconnection is a fundamental plasma process whereby magnetic energy is rapidly and efficiently converted into plasma flows, heating, and potentially non-thermal particles [1]. It plays a critical role in the evolution of magnetized plasmas in space physics, astrophysics and laboratory nuclear fusion devices [2–4]. Energetic particles are a common signature of the reconnection process, and reconnection is thought to be a promising candidate for producing the non-thermal emissions associated with explosive phenomena such as solar flares, pulsar wind nebulae and jets from active galactic nuclei. These systems span a large range of plasma conditions, and many recent studies have focused on understanding the details of the particle acceleration in both nonrelativistic [5–9] and relativistic [10, 11] regimes. These studies have discovered a rich variety of acceleration mechanisms, with many mediated by the plasmoids that can form in the current sheet due to the tearing instability [12]. The overall efficiency of reconnection in producing energetic particles and its dependence on the plasma conditions, however, has not been settled, and thus remains an important and active area of research.

Recently, laser-driven high-energy-density (HED) plasmas have started to be used to study reconnection in the laboratory [13–19] (for a review of laboratory reconnection experiments see [20]). By focusing terawatt class ($\sim$kJ/ns) lasers onto solid foils, plasma bubbles are produced that expand and generate megagauss scale toroidal magnetic fields by the Biermann battery ($\nabla n \times \nabla T$) mechanism [21]. The expansion of two bubbles placed in close proximity can then drive reconnection between the self-generated or externally imposed [19] magnetic fields (Figure 1(a)). Many of the prominent features of reconnection have been observed in these systems, including plasma jets, plasma heating, changes in magnetic field topology, and plasmoid formation. Supersonic and super-Alfvénic inflow speeds place these experiments in a regime of strongly-driven reconnection, making them particularly relevant for systems featuring colliding magnetized plasma flows found in space and astrophysics. Laser-driven plasma experiments are characterized by a high Lundquist number and large system size relative to the electron and ion inertial lengths, allowing a comparison with astrophysical systems via scaling laws [22]. Until now, the possibility of using laser-driven plasmas to study non-thermal particle acceleration induced by reconnection has remained unclear.

In this Letter, we investigate the onset and the properties of particle acceleration during reconnection in laser-driven plasmas using *ab initio* particle-in-cell (PIC) simulations. Using

2

the fully relativistic, state-of-the-art PIC code OSIRIS [23–26] we perform two-dimensional (2D) and, for the first time, three-dimensional (3D) simulations in realistic experimental conditions and geometries. We demonstrate the possibility of detecting electrons with energies more than an order of magnitude larger than the thermal energy in conditions relevant to current experiments. The electrons are accelerated primarily by the reconnection electric field, with the randomness associated with injection at varied distances from the X-points and escape from the finite-sized system leading to a non-thermal component with a power-law shape. Furthermore, a fraction of the electrons can be trapped in plasmoids, slowly gaining further energy due to the drifting motion of the plasmoid. An estimate for the maximum electron energy and a threshold condition for suprathermal energization are given in terms of experimentally tunable parameters, which can guide future studies of particle acceleration induced by reconnection in laser-driven plasmas.

We simulate the interaction between two expanding, magnetized plasma bubbles, consistent with previous PIC studies [27–30] (Figs. 1(b) and 1(c)). The simulations start when the bubbles are about to interact, and thus do not model the initial generation of the plasma or magnetic field. However, they capture the most important features of the system such as finite size and driven inflows, allowing them to be connected to a number of experimental geometries [31]. The bubbles are centered at $\mathbf{R}^{(1)} = (0, R, 0)$ and $\mathbf{R}^{(2)} = (0, -R, 0)$, with the radial vectors from the bubble centers being $\mathbf{r}^{(i)} = \mathbf{r} - \mathbf{R}^{(i)}$. Here R is the radius of each bubble when they begin to interact. The initial density profile is $n_b + n^{(1)} + n^{(2)}$ where $n^{(i)}(r^{(i)}) = (n_0 - n_b)\cos^2\left(\frac{\pi r^{(i)}}{2R_0}\right)$ if $r^{(i)} < R_0$, 0 otherwise. Here, $n_b = 0.01 n_0$ is a background plasma density, and R_0 is the initial bubble radius, which we typically take to be $0.9 - 1.0R$. The velocity profile is $\mathbf{V}^{(1)} + \mathbf{V}^{(2)}$ where $\mathbf{V}^{(i)}(r^{(i)}) = V_0 \sin\left(\frac{\pi r^{(i)}}{R_0}\right) \mathbf{r}^{(i)}$ if $r^{(i)} < R_0$, 0 otherwise. The initial magnetic field is divergence free and corresponds to the sum of two oppositely aligned ribbons, $\mathbf{B}^{(1)} + \mathbf{B}^{(2)}$ where $\mathbf{B}^{(i)}(r^{(i)}) = B_0 f(\theta^{(i)}) \sin\left(\frac{\pi(R_0 - r^{(i)})}{2L_B}\right) \hat{\phi}^{(i)}$ if $R_0 - 2L_B \leq r^{(i)} \leq R_0$, 0 otherwise. $L_B = R_0/4$ is the initial half-width of the magnetic field ribbon. $\theta^{(i)}$ and $\phi^{(i)}$ are the polar and azimuthal angles, respectively, of spherical coordinate systems originating at the bubble centers. For the 2D simulations, which model the plane $\theta^{(i)} = \pi/2$, $f(\theta^{(i)}) = 1$. For the 3D simulations, $f(\theta^{(i)})$ is zero near the z-axis, rises from 0 to 1 from $\theta^{(i)} = \pi/16$ to $\theta^{(i)} = 2\pi/16$, and similarly from $\theta^{(i)} = 15\pi/16$ to $\theta^{(i)} = 14\pi/16$. The rise is given by the polynomial $10x^3 - 15x^4 + 6x^5$ which approximates a Gaussian shape. The motional electric field is initialized as $\mathbf{E} = -\mathbf{V} \times \mathbf{B}/c$, where $\mathbf{V} = \mathbf{V}_e = \mathbf{V}_i$

3

at $t = 0$. The 2D (3D) simulations use a box of size $8R \times 2R$ ($4R \times 2R \times 4R$) and are evolved to $t/t_d = 0.5(0.25)$, where $t_d = R/V_0$ is the relevant timescale for the interaction. The boundaries along the outflow directions are absorbing for the particles initially in the plasma bubble, thermal re-emitting for the particles initially in the background plasma, and an absorbing layer [32] for the electromagnetic fields. The energy spectra presented are integrated over the electrons initially in the bubbles. Simulations with larger domains confirm that the boundaries are not affecting the results. Periodic boundaries are used along the inflow direction, taking advantage of the antisymmetry of the system. We note that the majority of reconnection simulation studies employ periodic boundaries in the direction of the reconnection outflows and thus may suffer unphysical effects from recirculating particles and radiation. Studying particle acceleration in the finite-sized systems of laser-driven plasmas would yield critical insight for understanding the role of boundary conditions and particle escape in models of reconnection.

To directly match laboratory conditions of interest (e.g. those generated with the OMEGA EP laser [19]) we model a range of Alfvénic and sonic Mach numbers, $M_A = V_0/V_A = 4 - 64$ and $M_S = V_0/C_S = 2 - 8$, where $V_A = B_0/\sqrt{4\pi n_0 m_i}$ is the Alfvén speed and $C_S = \sqrt{Z T_e/m_i}$ is the sound speed. We also match the high experimental plasma beta, $\beta_e = \frac{n_0 T_e}{B_0^2/8\pi} = 2\left(\frac{M_A}{M_S}\right)^2 = 8 - 128$. The bubble radii are $R/(c/\omega_{pi}) \simeq 26.5\,(20)$ for the 2D (3D) simulations, within the experimentally accessible range of $R/(c/\omega_{pi}) = 10 - 100$ [28]. The initial temperatures T_e and T_i are taken to be equal and uniform. The parameters C_S/c and $m_i/m_e Z$ (where c is the speed of light, m_i and m_e the ion and electron masses, and Z the ion charge) are not directly matched to experimental values due to computational expense. In the majority of the simuations we use $V_0/c = 0.1$ and $m_i/m_e Z = 128$, with C_S chosen to correctly match M_S. By varying these parameters in the range $V_0/c = 0.025 - 0.1$ and $m_i/m_e Z = 32 - 512$ we have verified that the main results of this study are relatively insensitive to their exact values. All simulations use a spatial grid of resolution of $\Delta x = 0.5 c/\omega_{pe} \simeq 0.04 c/\omega_{pi}$ and cubic interpolation for the particles. The 2D (3D) simulations use a timestep of $\Delta t = 0.35(0.285)\,\omega_{pe}^{-1}$ and 64 (8) particles per cell per species.

We first analyze in detail the 2D simulation with $M_S = 2$ and $M_A = 4$. We observe that the early evolution of the system is consistent with previous studies using this configuration [27–30]. As the plasma flows bring in the magnetic flux at super-Alfvénic speeds, the plasma is compressed by the ram pressure and the amplitude of the magnetic field increases by a

factor of ≈ 1.65. A current sheet forms on the order of the ion inertial length, which is the scale at which electrons and ions decouple, enabling fast reconnection mediated by the Hall effect [34]. The current sheet is then unstable to the tearing instability, and we observe the formation of a single plasmoid, consistent with linear theory which predicts $k_{max}\delta = 0.55$, where $\delta \approx 1.41\,c/\omega_{pi}$ is the half-width of the current sheet [33]. For the range of conditions simulated we typically observe magnetic field enhancement by a factor of 1.5 to 5 and the formation of 1-3 plasmoids. The calculation of the different terms in the generalized Ohm's law ($\mathbf{E} = -\frac{1}{c}\frac{n_i}{n_e}\mathbf{v}_i \times \mathbf{B} + \frac{1}{en_ec}\mathbf{J} \times \mathbf{B} - \frac{\nabla\cdot\mathbf{P}_e}{en_e} - \frac{m_e}{e}\frac{d\mathbf{v}_e}{dt}$) shows that the electric field in the diffusion region is predominantly supported by the Hall and off-diagonal electron pressure tensor terms, in agreement with previous kinetic studies of reconnection starting from the Harris equilibrium [34] and laser-driven reconnection [27]. For the geometry of our configuration the typical value of the reconnection electric field in the diffusion region is $E \approx 0.5V_0B_0$ (Figure 1(c)). In terms of the local Alfvén speed and compressed magnetic field, we find $E \approx 0.3V_AB$ at $t/t_d = 0.25$, when the plasmoid is just beginning to form. After the onset of reconnection, the finite size of the plasma bubbles results in reconnection outflows that are directed out of the interaction region.

Figure 1(d) shows the temporal evolution of the electron energy spectrum for this simulation. We observe the development of a non-thermal component with energies up to $\approx 50\,k_BT_e$ that resembles a power law with index $P \approx -5.3$. In Figure 2(a), a distribution of energetic electrons is seen in the reconnection region. The energy decreases with distance from x = 0, which is approximately the location of the X-point before the plasmoid forms. At a later time, shown in Figure 2(b), energetic electrons are seen both to escape in the plasma outflows and to be trapped in a peak at the location of the single plasmoid that forms in the simulation. The most energetic electrons are trapped at $t/t_d = 0.5$. In a realistic 3D system, which we will discuss later, the trapped electrons would also escape the reconnection region, but along the z-direction.

In order to understand the details of the particle acceleration, we tracked the detailed motion of the most energetic electrons in the simulation. The relative importance of the electric field components in energizing the electrons was determined by calculating the work done by each throughout the simulation, $W_i = \int_0^t dt'(p_i/\gamma\,m_e)(-e\,E_i)$. Figs. 2(c) and 2(d) show trajectories that illustrate the two distinct types of behavior observed for the energetic electrons. The evolution of the total energy and the work done by the electric field

components for these electrons is plotted in Figs. 2(e) and 2(f). In both cases the particles gain the majority of their energy as they are accelerated in the out-of-plane direction by the reconnection electric field near the X-point, as can be seen in the insets in Figs. 2(c) and 2(d). The in-plane magnetic field then rotates the velocities of the electrons into the plane, at which point the electrons will either escape in the outflow direction (as in Figure 2(c)), become trapped in a plasmoid (as in Figure 2(d)), or travel around the bubble along the field lines. The electrons that escape the reconnection region lose some of their energy to the in-plane polarization electric field (Figure 2(e)), whereas the trapped electrons can be further accelerated due to the motion of the plasmoid. The energization rate is seen to decrease for the trapped electrons, as shown in Figure 2(f). In this simulation the plasmoid is slowly drifting along the outflow direction, and thus the trapped electrons see an out-of-plane motional electric field with alternating polarity (Figure 1(c)) as they circle inside the plasmoid [5]. Plasma flowing into the drifting plasmoid from the bounding X-points leads to an asymmetry in its motional electric field, allowing trapped electrons to gain further energy. Simulations with a single bubble confirm that the electric field from the bubble expansion does not significantly energize particles.

In Figure 3(a) we observe that the low-energy portion of the electron distribution is well fitted by a Maxwell-Boltzmann distribution (blue dashed line) and that there is a non-thermal component that starts at $\sim 5k_BT_e$ and resembles a power-law with an index of ~ 5.3 and an exponential cutoff at $\sim 20k_BT_e$ (red dashed line). Periodic simulations for the same plasma parameters but transversely infinite profiles (not shown here) show that in much larger systems the power-law component extends to higher energies and has a harder index of ~ 3.5, indicating the importance of particle escape in finite systems. The comparison with transversely infinite systems will be discussed in detail elsewhere. At the end of the simulation ($t/t_d = 0.5$), the non-thermal component contains $\sim 8\%$ of the initial energy of interacting electrons, $\sim 24\%$ of the initial energy stored in the magnetic field, and $\sim 1\%$ of the total number of electrons initially in the bubbles. Previous work has shown that the presence of plasmoids may give rise to Fermi-acceleration mechanisms [8]. Calculating $d\epsilon/dt$ as a function of ϵ for the tracked particles (where ϵ is energy) shows an energization rate that is approximately constant, indicating that the dominant acceleration mechanism producing the energetic electrons is not Fermi acceleration. This is likely to require a much larger number of plasmoids and thus a more energetic laser drive than that used in current

experiments. We note that even in the simulations with up to 3 plasmoids we do not observe evidence of Fermi acceleration associated with the plasmoids. In our case, the distribution of energies for the accelerated electrons is established as electrons are injected into the diffusion region at varied distances from the X-points and escape the diffusion region at different times. The electrons that interact nearer to the X-point are exposed to the reconnection electric field for a longer amount of time before the in-plane magnetic fields direct them out of the diffusion region, allowing them to reach higher energies [11]. Additional randomness is introduced by the finite probability for a given electron to escape from the system or become trapped in a plasmoid and further energized.

Figure 3(b) shows a comparison of the electron energy spectra at $t/t_d = 0.25$ for four 2D simulations with $M_S = 2$ and M_A ranging from 4 to 32. All show the development of a high energy tail with a power-law shape and similar spectral indices, indicating the similarity of the acceleration mechanisms across these conditions. The maximum electron energy attained increases with the initial magnetic field amplitude, consistent with the picture that the electrons gain their energy directly from the reconnection electric field. Figure 3(c) shows the evolution of the maximum electron energy in each simulation, and the corresponding energization rates are shown in Figure 3(d). The effective electric field corresponding to the energization rate is found to be close to $0.5V_0 B_0$ for all cases, consistent with the typical value of the reconnection electric field observed in the diffusion region in the simulations.

2D simulations do not capture the finite size of the system in the out-of-plane (acceleration) direction. It is thus critical to consider 3D effects. To this end we have performed full 3D simulations of reconnection between expanding plasma bubbles, with the initialization described above and the conditions $M_S = 2, M_A = 4$. They show that the out-of-plane variation does not significantly change the acceleration picture but does limit the maximum electron energy attainable. An important difference to the 2D case is the fact that the amplitude of the magnetic field is only seen to increase by $\approx 7\%$, in contrast with the $\approx 65\%$ increase in 2D. The electron spectrum at $t/t_d = 0.25$ is shown in Figure 3(b). The spectrum exhibits a high-energy tail with a similar spectral index to the 2D case, demonstrating that the non-thermal energization survives in 3D and that the acceleration mechanisms are similar. The maximum electron energy is smaller for the 3D case, due to the finite out-of-plane size limiting the maximum energy attainable. The energization rate is also slightly smaller in 3D, due to the fact that the electrons do not see a uniform value of the reconnection

7

electric field as they travel in the out-of-plane direction.

The finite out-of-plane size limits the distance over which an electron can be accelerated by the reconnection electric field to approximately the diameter of the bubble. Considering the effective value of the reconnection electric field is $\approx 0.5 V_0 B_0$, an estimate for the maximum energy increase of an electron can then be written in terms of experimentally tunable parameters as $\epsilon_{max}/k_B T_e = (M_S^2/M_A)(R_b/(c/\omega_{pi}))$. Applying this to the parameters of the 3D simulation presented above gives $\epsilon_{max}/k_B T_e \approx 20$, which predicts well the location of the exponential cutoff of the power-law as shown in Figure 3(b). The threshold condition for producing suprathermal electrons in the laboratory is then $(M_S^2/M_A)(R_b/(c/\omega_{pi})) > 1$, which is easily satisfied by the conditions accessible in current experiments. The conditions of two recent laser-driven reconnection experiments at the Omega Laser Facility [19, 28] are estimated to be $M_S \approx 2.5, 5.6$, $M_A \approx 20, 9.2$, and $R_b/(c/\omega_{pi}) \approx 80, 22$. For these conditions our model predicts maximum electron energies of $\epsilon_{max}/k_B T_e \approx 25, 75$. An important experimental signature of this acceleration due to reconnection is that the non-thermal electrons should be detected in a fan-like profile, with energetic electrons being emitted both in the direction of reconnection outflows and in the direction opposite to the reconnection electric field.

In summary, by performing *ab initio* kinetic simulations of magnetic reconnection in laser-driven plasmas, we have shown that these systems can accelerate non-thermal electrons to energies more than an order of magnitude larger than the thermal energy in conditions currently accessible in the laboratory. Electron injection at varied distances from the X-points and escape from the finite-sized system leads to a non-thermal component that resembles a power-law spectrum. Our results indicate that laser-driven plasmas thus offer a new platform for the experimental study of particle acceleration induced by reconnection, which could help illuminate the role reconnection plays in explosive phenomena associated with space and astrophysical plasmas.

---

* fiuza@slac.stanford.edu

[1] E. G. Zweibel and M. Yamada, Annual Review of Astronomy and Astrophysics **47**, 291 (2009).

[2] H. Ji and W. Daughton, Physics of Plasmas **18**, 1 (2011), arXiv:1109.0756.

[3] A. S. Joglekar, A. G. R. Thomas, W. Fox, and A. Bhattacharjee, Physical Review Letters **112**, 1 (2014).

[4] J. B. Taylor, Reviews of Modern Physics **58**, 741 (1986).

[5] M. Oka, T.-D. Phan, S. Krucker, M. Fujimoto, and I. Shinohara, The Astrophysical Journal **714**, 915 (2010), arXiv:1004.1154.

[6] X. R. Fu, Q. M. Lu, and S. Wang, Physics of Plasmas **13**, 1 (2006).

[7] M. Hoshino, T. Mukai, T. Terasawa, and I. Shinohara, Journal of Geophysical Research **106**, 25979 (2001).

[8] J. F. Drake, M. Swisdak, H. Che, and M. A. Shay, Nature **443**, 553 (2006).

[9] J. T. Dahlin, J. F. Drake, and M. Swisdak, Physics of Plasmas **092304**, 19 (2014), arXiv:1406.0831.

[10] F. Guo, H. Li, W. Daughton, and Y.-H. Liu, Physical Review Letters **155005**, 4 (2014), arXiv:1405.4040.

[11] L. Sironi and A. Spitkovsky, The Astrophysical Journal **783**, L21 (2014), arXiv:1401.5471.

[12] N. F. Loureiro, A. A. Schekochihin, K. College, and S. C. Cowley, Physics of Plasmas **14**, 14 (2007), arXiv:0703631 [astro-ph].

[13] P. M. Nilson, L. Willingale, M. C. Kaluza, C. Kamperidis, S. Minardi, M. S. Wei, P. Fernandes, M. Notley, S. Bandyopadhyay, M. Sherlock, R. J. Kingham, M. Tatarakis, Z. Najmudin, W. Rozmus, R. G. Evans, M. G. Haines, A. E. Dangor, and K. Krushelnick, Physical Review Letters **97**, 1 (2006).

[14] C. K. Li, F. H. Séguin, J. A. Frenje, J. R. Rygg, R. D. Petrasso, R. P. J. Town, O. L. Landen, J. P. Knauer, and V. A. Smalyuk, Physical Review Letters **99**, 055001 (2007).

[15] P. M. Nilson, L. Willingale, M. C. Kaluza, C. Kamperidis, S. Minardi, M. S. Wei, P. Fernandes,

M. Notley, S. Bandyopadhyay, M. Sherlock, R. J. Kingham, M. Tatarakis, Z. Najmudin, W. Rozmus, R. G. Evans, M. G. Haines, A. E. Dangor, and K. Krushelnick, Physics of Plasmas **15**, 092701 (2008).

[16] L. Willingale, P. M. Nilson, M. C. Kaluza, A. E. Dangor, R. G. Evans, P. Fernandes, M. G. Haines, C. Kamperidis, R. J. Kingham, C. P. Ridgers, M. Sherlock, a. G. R. Thomas, M. S. Wei, Z. Najmudin, K. Krushelnick, S. Bandyopadhyay, M. Notley, S. Minardi, M. Tatarakis, and W. Rozmus, Physics of Plasmas **17**, 043104 (2010).

[17] J. Zhong, Y. Li, X. Wang, J. Wang, Q. Dong, C. Xiao, S. Wang, X. Liu, L. Zhang, L. An, F. Wang, J. Zhu, Y. Gu, X. He, G. Zhao, and J. Zhang, Nature Physics **6**, 984 (2010).

[18] Q. L. Dong, S. J. Wang, Q. M. Lu, C. Huang, D. W. Yuan, X. Liu, X. X. Lin, Y. T. Li, H. G. Wei, J. Y. Zhong, J. R. Shi, S. E. Jiang, Y. K. Ding, B. B. Jiang, K. Du, X. T. He, M. Y. Yu, C. S. Liu, S. Wang, Y. J. Tang, J. Q. Zhu, G. Zhao, Z. M. Sheng, and J. Zhang, Physical Review Letters **108**, 1 (2012), arXiv:arXiv:1203.4036v1.

[19] G. Fiksel, W. Fox, A. Bhattacharjee, D. H. Barnak, P.-Y. Chang, K. Germaschewski, S. X. Hu, and P. M. Nilson, Physical Review Letters **113**, 1 (2014).

[20] M. Yamada, R. Kulsrud, and H. Ji, Reviews of Modern Physics **82**, 603 (2010).

[21] M. Haines, Physical Review Letters **78**, 254 (1997).

[22] D. D. Ryutov, R. P. Drake, and B. A. Remington, The Astrophysical Journal Supplement Series **127**, 465 (2000).

[23] R. G. Hemker, (2015), arXiv:1503.00276.

[24] R. Fonseca, L. Silva, and F. Tsung, ScienceICCS 2002 , 342 (2002).

[25] R. A. Fonseca, S. F. Martins, L. O. Silva, J. W. Tonge, F. S. Tsung, and W. B. Mori, Plasma Physics and Controlled Fusion **124034**, 10 (2008), arXiv:0810.2460.

[26] R. A. Fonseca, J. Vieira, F. Fiuza, A. Davidson, F. S. Tsung, W. B. Mori, and L. O. Silva, Plasma Physics and Controlled Fusion **55**, 124011 (2013), arXiv:1310.0930.

[27] W. Fox, A. Bhattacharjee, and K. Germaschewski, Physical Review Letters **106**, 215003 (2011), arXiv:1104.0605.

[28] W. Fox, A. Bhattacharjee, and K. Germaschewski, Physics of Plasmas **19** (2012), 10.1063/1.3694119.

[29] S. Lu, Q. Lu, Q. Dong, C. Huang, S. Wang, J. Zhu, Z. Sheng, and J. Zhang, Physics of Plasmas **20**, 112110 (2013).

[30] S. Lu, Q. Lu, C. Huang, Q. Dong, J. Zhu, Z. Sheng, S. Wang, and J. Zhang, New Journal of Physics **16**, 083021 (2014).

[31] D. D. Ryutov, N. L. Kugland, M. C. Levy, C. Plechaty, J. S. Ross, and H. S. Park, Physics of Plasmas **20**, 032703 (2013).

[32] J.-L. Vay, Journal of Computational Physics **165**, 511 (2000).

[33] P. L. Pritchett, F. V. Coroniti, R. Pellat, and H. Karimabadi, Journal of Geophysical Research **96** (1991), 10.1029/91JA01094.

[34] P. L. Pritchett, "Geospace Environment Modeling magnetic reconnection challenge: Simulations with a full particle electromagnetic code," (2001).
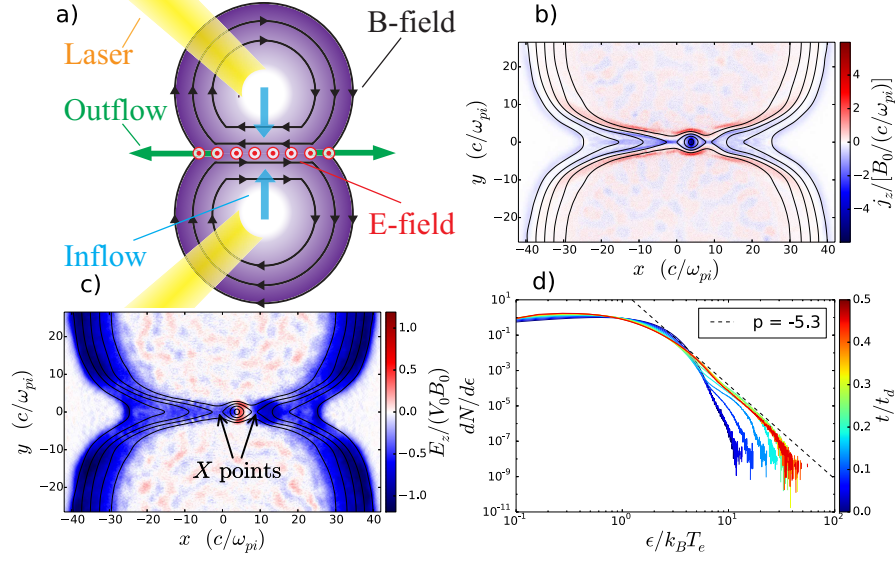
FIG. 1. a) Geometry of laser-driven reconnection experiments and simulations. b) Out-of-plane current density and c) Out-of-plane electric field, with overlayed magnetic field lines. At the X-points, this is the reconnection electric field. d) Evolution of the electron energy spectrum.
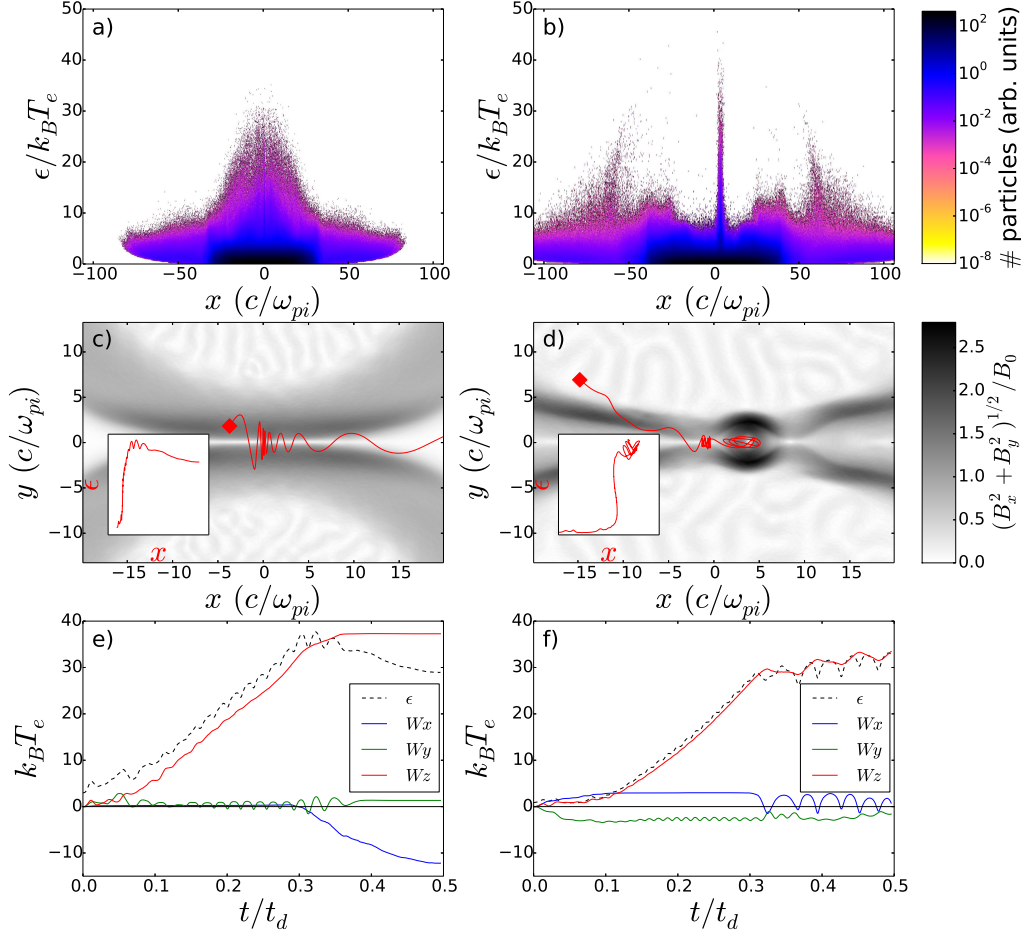
FIG. 2. a), b) Electron energy spectrum along the x-direction at $t/t_d = 0.25, 0.5$, respectively. c) Trajectory of an escaping electron and d) Trajectory of a trapped electron, plotted over the magnitude of the in-plane magnetic field at $t/t_d = 0.25, 0.5$, respectively. Diamonds indicate the particle's position at $t = 0$, and insets show the energy variation of the particle along x. e), f) Evolution of the total energy and work done by the electric field components for the electrons shown in c), d), respectively.
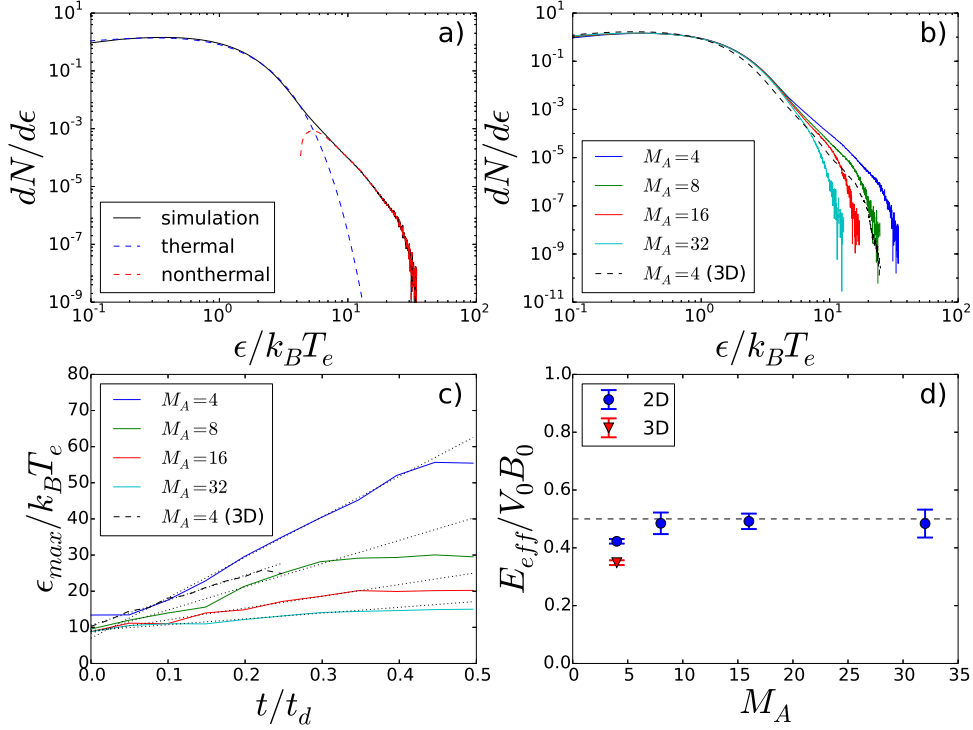
FIG. 3. a) Electron energy spectrum for the $M_S = 2$, $M_A = 4$ simulation at $t/t_d = 0.25$, with the thermal component (blue dashed line) and the non-thermal component (red dashed line). b) Comparison of the electron energy spectra for different M_A in 2D and 3D at $t/t_d = 0.25$. c) Temporal evolution of the maximum electron energy for the same simulations as in b), with linear fits plotted as dotted lines. d) Effective electric field obtained from the data in c). Error bars show the one standard deviation error obtained from the linear fit.